

Post-Yielding Stress-Strain Determination Using Spherical Indentation

B. S.-J. Kang, Z. Yao, and E. J. Barbero

Department of Mechanical and Aerospace Engineering, West Virginia University, Morgantown, WV, USA

In this research, finite element (FE) simulations were performed to verify Tabor's empirical relations that enable the use of the indentation test for determination of post-yielding uniaxial stress-strain curves of a variety of ductile metallic alloys. Both piling-up and sinking-in materials are included in this study. From the FE spherical indentation simulations, the indentation loads and projected contact radii are obtained for various elastic power-law plastic solids in both bulk and thin film substrate systems. It is found that for bulk materials, the indentation stresses and strains obtained from Tabor's empirical formula agreed well with the input uniaxial stress-strain data. This approach is then verified experimentally by spherical indentation tests on Inconel 783 alloy. In thin film substrate system, two cases, soft film on hard substrate and hard film on soft substrate were studied and the substrate effect on Tabor's relation was analyzed.

1. INTRODUCTION

In recent years, instrumented spherical indentation [1–4, 11] has been studied and developed as an effective, non-destructive method to evaluate surface mechanical properties of metallic materials. This technique is applicable in cases where a traditional material tension test cannot be conducted. The goal is to correlate the experimental indentation data, i.e., load and indentation depth, to material mechanical properties such as elastic modulus and post-yielding strain hardening. Based on Sneddon's analytical solution [5] for linear elastic materials and the assumption that the unloading of indentation is pure elastic rebound of the material, the elastic modulus can be extracted from the initial unloading part of load-depth curve [6, 7]. The accuracy of this technique has been proved by both experiments [8] and numerical methods [9]. However, it is difficult to correlate the post yielding behavior with indentation data analytically since the governing constitutive relationship is nonlinear and a complex 3-D state of stress is induced under the indenter.

In Tabor's empirical work [10], it was pointed out that for spherical indentation, Meyer's hardness, which was defined as the mean contact pressure $p_m = \frac{P}{A_{proj}}$, has a close agreement

with the uniaxial stress-strain curve. The Tabor empirical formulas of indentation stress and strain are

$$\begin{cases} \varepsilon_i = 0.2 \frac{d}{D} \\ \sigma_i = \frac{p_m}{2.8} \end{cases} \quad (1)$$

where d is the indentation impression diameter, D is the ball indenter diameter, Tabor showed that the indentation stress-strain relation (Eq. (1)) is equal to the uniaxial compression stress-strain curve in the fully plastic region, as shown in Figure 1. Such conclusion was based on experiments on two alloys: mild steel and anneal copper. It was also pointed out that this relationship is independent of the indenter size [10].

It should be noted that the indentation stress and strain obtained based on Eq. (1) are averaged values beneath the indenter. The determination of the coefficients 0.2 and 2.8 in Eq. (1) is empirical and arbitrary. For instance, Jeong-Hoon Ahn et al. [11] proposed four kinds of strain definitions and determined $\sigma_i = p_m/3$.

In this research, FE simulations are performed to verify Tabor's empirical relation. Twenty-one linear elastic, power-law plastic material models are selected. The indentation data (contact radius and load) are extracted from the FE simulation results. Computed stress/strain data based on Eq. (1) are compared with the input stress-strain data. The fully plastic condition to apply Tabor's equation is also evaluated quantitatively.

The same concept is applied to materials with thin film coating. Two configurations of thin film substrate system, soft film on hard substrate and hard film on soft substrate, are analyzed and the effect of substrate on both cases is studied.

2. MATERIAL MODELS

It is assumed that uniaxial true stress-strain curve follows piecewise linear elastic—power-law plastic model

$$\varepsilon = \begin{cases} \sigma/E & \sigma < \sigma_y \\ \frac{\sigma_y}{E} \left(\frac{\sigma}{\sigma_y} \right)^{1/n} & \text{otherwise} \end{cases} \quad (2)$$

or

$$\sigma = \begin{cases} E\varepsilon & \sigma < \sigma_y \\ \sigma_y \left(\frac{E}{\sigma_y} \right)^n \varepsilon^n & \text{otherwise} \end{cases}$$

Received 27 October 2004; accepted 26 October 2005.

Address correspondence to B. S.-J. Kang, Department of Mechanical and Aerospace Engineering, West Virginia University, Morgantown, WV 26506-6106. E-mail: bruce.kang@mail.wvu.edu

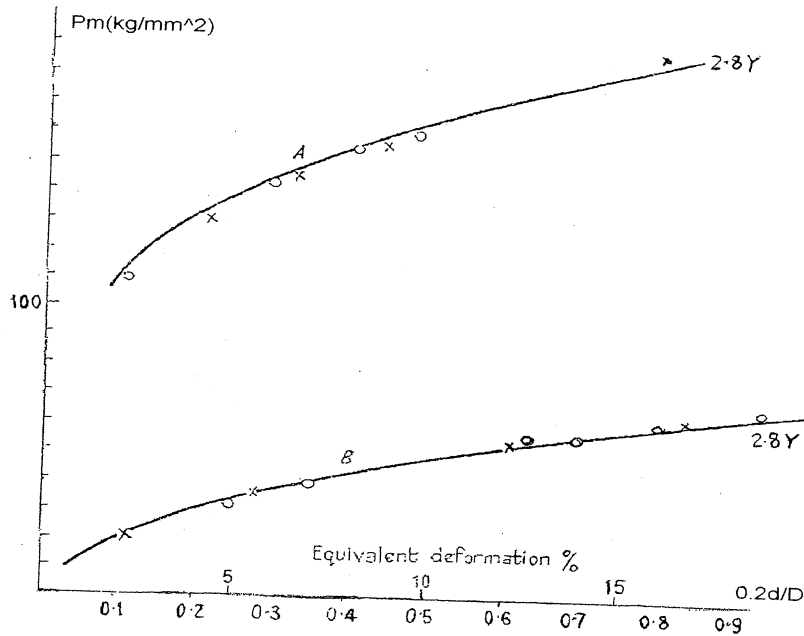


FIG. 1. Tabor's experimental results: comparison of hardness measurements with the stress-strain curve. A, mild steel. B, annealed copper [10].

in which three parameters, Young's modulus, E , Yield Stress, σ_y , and power hardening exponent, n , are used to determine the material stress-strain curve. This equation accurately describes the elastic regime of metallic materials and their subsequent plastic strain hardening behavior through a power-law relation. The latter provides a good approximation to the stress-strain curve of metals at least to intermediate values of plastic deformation. Also, it is formulated in such a way that the elastic behavior matches the plastic response at $\sigma = \sigma_y$. The existence of such well-defined yield strength allows one to model the response of metallic materials when subjected to different amounts of strain hardening [12]. For general elastic plastic materials, the n value lies between 0 and 1. This material model has been applied to many numerical indentation simulation studies [12, 13].

For this research, three sets of bulk engineering alloys are selected: aluminum alloys, steel alloys and lead free solder materials, as shown in Table 1.

Twenty-one materials are simulated, which span from soft material (lead free solder material) to relatively strong material (steel alloy). For a designated set of material, the Young's modulus varies in a limited range (e.g., for aluminum alloys $E = 69$ GPa, for steel alloys $E = 200$ GPa), while the σ_y and n values are in a wide range due to different composition and heat treatment of the alloys. For thin film substrate systems, two basic materials, aluminum and silicon, are selected with two arrangements; soft film (Al) on hard substrate (Si) and hard film (Si) on soft substrate (Al). The material properties are listed in Table 2. The film thickness is kept at $30 \mu\text{m}$.

TABLE 1
Simulation matrix: Material library selection

Aluminum alloys ($E = 69$ GPa, $\nu = 0.33$)									
$\sigma_y = 275$ MPa (6061-T6)					$\sigma_y = 500$ MPa (7075-T651)				
$n = 0.09$	$n = 0.18$	$n = 0.27$	$n = 0.36$	$n = 0.09$	$n = 0.18$	$n = 0.27$	$n = 0.36$		
Steel ($E = 200$ GPa, $\nu = 0.3$)									
$\sigma_y = 242$ MPa (mild steel)			$\sigma_y = 500$ MPa				$\sigma_y = 750$ MPa		
$n = 0.1$	$n = 0.2$	$n = 0.3$	$n = 0.1$	$n = 0.2$	$n = 0.3$	$n = 0.1$	$n = 0.2$	$n = 0.3$	
Lead free solder materials ($E = 26.2$ GPa, $\nu = 0.3$)									
$\sigma_y = 22.5$ MPa (Sn-3.5Ag)									
$n = 0.026$		$n = 0.1$		$n = 0.2$		$n = 0.3$			

TABLE 2
Material properties used for finite element simulations in thin film cases

	Young's modulus (GPa)	Poisson's ratio	Yield stress (MPa)	Strain hardening exponent
Silicon	127	0.278	4410	0
Aluminum	69	0.33	275	0.09

Relatively small indenter ($D = 100 \mu\text{m}$) is used in these cases.

3. FINITE ELEMENT MODELING

FE indentation simulations were performed for the problem of a rigid spherical indenter pushed into contact against the half space using ABAQUSTM [14]. The constitutive model of the half space is taken to follow J_2 -associated flow theory with rate-independent deformation and isotropic hardening. The von Mises yield criterion is applied in the FE computations. The process of indentation is assumed to be quasi-static and no rate effects are represented. To spare CPU time, a two-dimensional axisymmetric model is employed. At first, the indenter is assumed to be perfectly rigid and is modeled as a rigid axisymmetric surface. For the mesh representing half space solid, a total of 21,573 four-node axisymmetric linear quadrilateral elements are utilized. Reduced integration is employed to minimize calculation time, while hourglass control is provided for this element type by ABAQUSTM. The region surrounding the indenter has fine mesh of 10,000 elements to model the high stress gradient and to obtain an accurate determination of the contact radius for the application of Eq. (1). To validate the convergence and adequate mesh design for the FE indentation simulations, a FE simulation with much finer mesh is performed and no significant deviation of the FE results is observed. Thus the adequacy of the mesh density shown in Figure 2 is validated.

To minimize the boundary effect, the total length of the FE mesh is twenty times larger than the sphere indenter radius. Two FE simulations with different boundary conditions were performed, as shown in Figures 3(a) and 3(b), and no significant difference was found. Thus it is concluded that the ratio of specimen size to the indenter size is large enough to simulate a small indenter being indented into half space solid. And the boundary condition has negligible effect on the simulation results.

Either the force applied to the indenter or the vertical displacement of the indenter tip could be used as input load. Almost identical results were obtained from either input mode. In this work, the displacement of the indenter tip is controlled. The force exerted on rigid indenter is then calculated by summation of y-direction reaction force of the bottom line nodes. The maximum depth of loading is 1/5 of the spherical indenter diameter for all simulations, which is $320 \mu\text{m}$ for bulk materials and $20 \mu\text{m}$ for thin film. In the FE modeling, the interface between the bilayer materials is assumed to be perfectly bonded and no interfacial fracture can occur during the process of indentation.

4. VERIFICATION OF THE FINITE ELEMENT MODEL

To verify the suitability of the FE mesh and modeling, elastic indentation simulations are first performed and solutions for load-depth curve are compared with the Hertz analytical solution. Since the analytical elastic solution is based on the assumption of small deformation, a relatively shallow indentation is simulated. The maximum indentation depth is $h_s = 10 \mu\text{m}$, using indenter diameter $D = 1.6 \text{ mm}$.

The analytical solution for load-depth relation of Hertz for perfectly rigid indenter indented on half space pure elastic specimen is given by

$$P = \frac{2\sqrt{2}}{3} \cdot \frac{E\sqrt{D}}{1-\nu^2} h_s^{3/2} \quad (3)$$

Excellent agreement between FE and Hertz analytical results are shown in Figure 4. It is also noticed that the load-depth

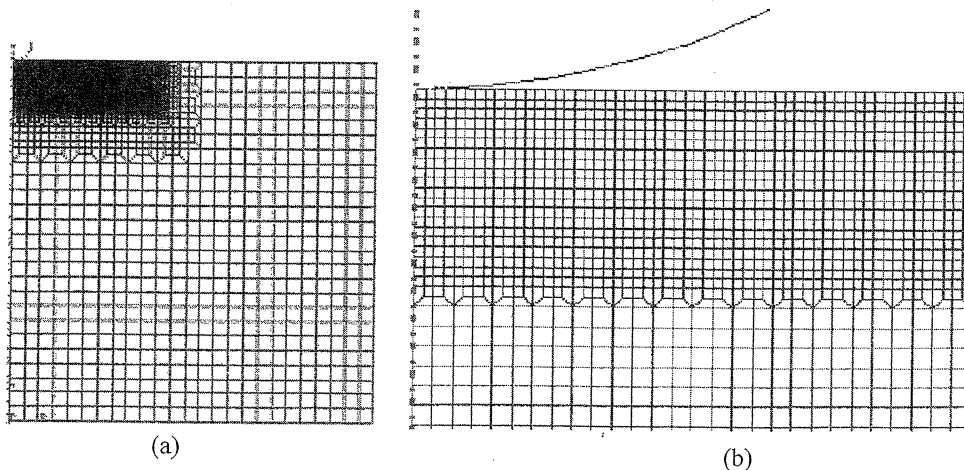


FIG. 2. (a) Mesh design (b) Magnified mesh design under indenter.

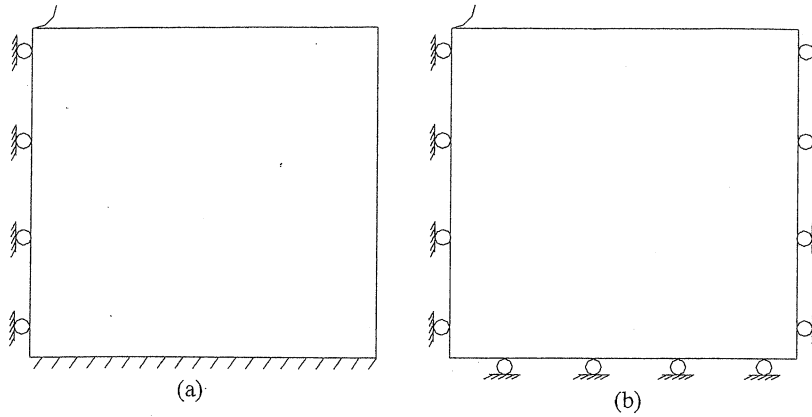


FIG. 3. (a) Fixed bottom, fixed side (b) Roller bottom, roller side.

curve fits better at the initial loading stage, as shown in Figure 5. This may be attributed to the gradual increase of numerical error caused by numerical integration to obtain the large deformation underneath the indenter.

In view of the favorable comparisons with the Hertz analytical solution, it may be concluded that the FE mesh and modeling assumptions are appropriate for simulating the indentation of a half-space by a rigid sphere.

5. BULK MATERIALS

To apply Tabor’s relation, two values are extracted from the simulation for every loading step: load, P , and contact radius, a . The projected contact area is: $A_{proj} = \pi a^2$. Due to the piling-up or sinking-in effect of the surface deformation, the contact radius cannot be directly derived from the indentation depth h_s , as shown in Figure 6.

The influence of the material properties on the surface deformation mode was discussed in detail in [15, 16]. Using a very fine mesh beneath the indenter, the contact radius can be obtained accurately. The progress of indentation is divided into three stages according to the response of the indented material: elastic, elastic-plastic, and fully plastic [10, 11]. This conclusion is verified from the FE simulations, as shown in Figure 7.

As pointed out by Tabor [1], Eq. (1) is only applicable under ‘fully plastic’ condition, which indicates relatively deep indentation. In Tabor’s work, it is claimed that full plasticity will be reached for mild steel when d/D is greater than 0.1 and for copper at a smaller value.

The boundary between the elastic-plastic regime and the fully plastic regime is determined by a nondimensional variable

$$\xi = E/\sigma_y \cdot \tan \gamma \tag{4}$$

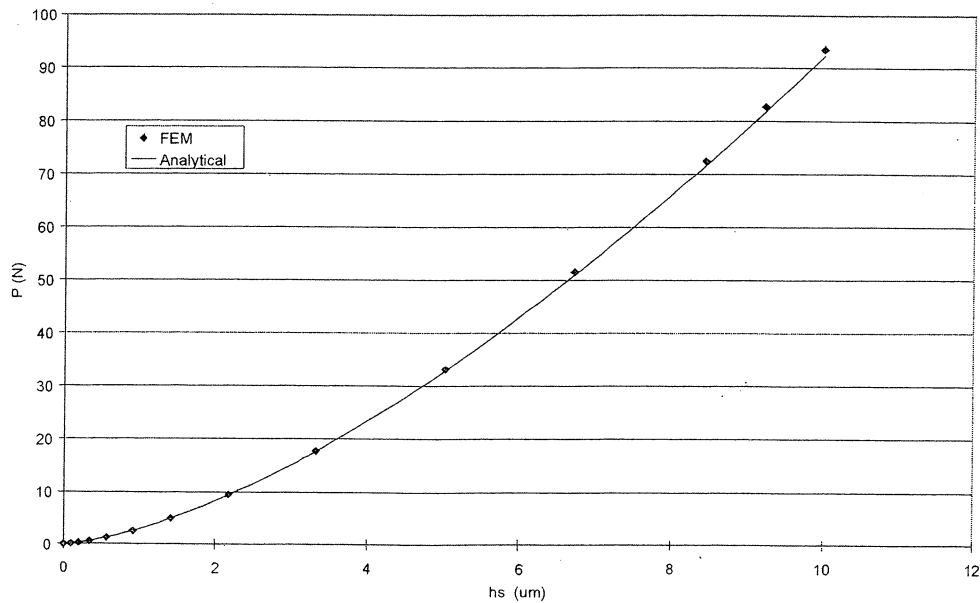


FIG. 4. Load depth curve comparison between FEM and analytical solution.

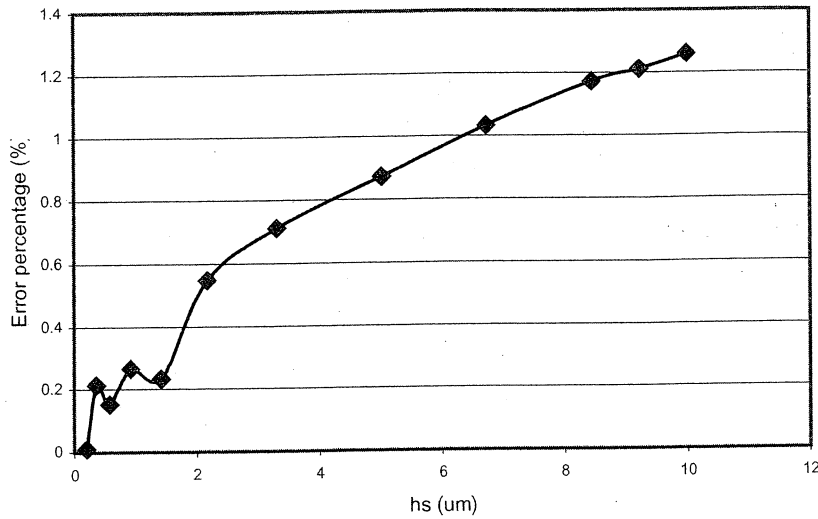


FIG. 5. Error percentage increases with indentation depth.

and its value is about 30 [17], where γ is the contact angle and it is calculated by

$$\sin \gamma = a/R = d/D \tag{5}$$

From the above analysis, the minimum strain value, which could be obtained from Tabor's relation, is

$$\epsilon_{\min} = 0.2 \sin[\tan^{-1}(30\epsilon_e)] \tag{6}$$

where $\epsilon_e = \sigma_y/E$ is the elastic strain at yielding.

As shown in Figures 8 to 13, good agreement between the Tabor's indentation stress-strain and input stress-strain curve for all the 21 material models is noted, with the maximum error less than 8%.

It is observed that for large n value ($n > 0.2$), Tabor's relation usually gives a higher value of stress especially at large plastic strains. The average of p_m/σ vs. n values is shown in Figure 14. As shown, the values of p_m/σ fluctuate between 2.82 to 2.98 for all 21 values of n , and thus support the validity of Tabor's relation in predicting post-yielding stress-strain behavior for metallic alloys. Based on Figure 9, however, it is proposed that the indentation stress should be modified as

$$\sigma_i = p_m/2.9 \tag{7}$$

while keeping the indentation strain unchanged.

It is difficult to measure the contact radius at maximum load experimentally. However, based on the assumption [15] that the contact radius does not change much during unloading process, the residual impression area, which could be measured directly using a microscope, is usually used to substitute for the contact area at maximum load. Direct observation from our FE simulations also verifies this assumption.

6. EXPERIMENTAL VERIFICATION

Spherical indentation test is implemented to verify the modified Tabor's relation. The material is Inconel 783 alloy with the mechanical property of $E = 177.3$ GPa, $\nu = 0.31$, $\sigma_y = 779$ MPa and $\sigma_{ult} = 1194$ MPa at 20% elongation. The stress-strain curve from uniaxial tensile test is shown in Figure 15.

A tungsten carbide ball indenter with $D = 1.6$ mm is used to conduct the indentation test on the Inconel 783 specimen. The load and corresponding residual impression diameter are recorded and the indentation stress-strain data are plotted to compare with the input stress-strain curve. The results are shown in Figure 15.

As shown, good agreement between the measured indentation stress-strain data and input stress-strain curve is noted. Thus, based on the modified Tabor formula, a simple indentation test procedure to obtain post-yielding stress-strain relationship of bulk materials is established.



FIG. 6. (a) piling-up mode (b) sinking-in mode.

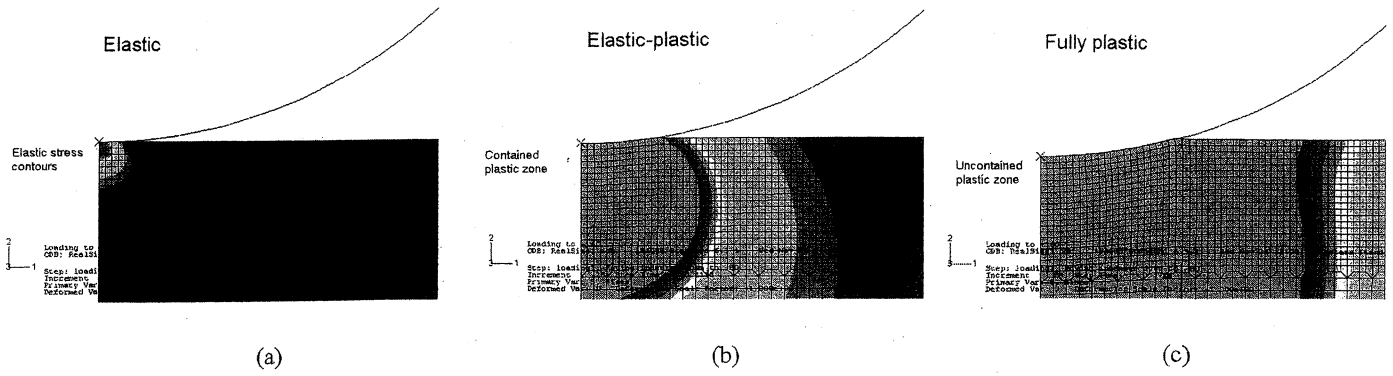


FIG. 7. (a) Elastic (b) Elastic-plastic (c) fully plastic.

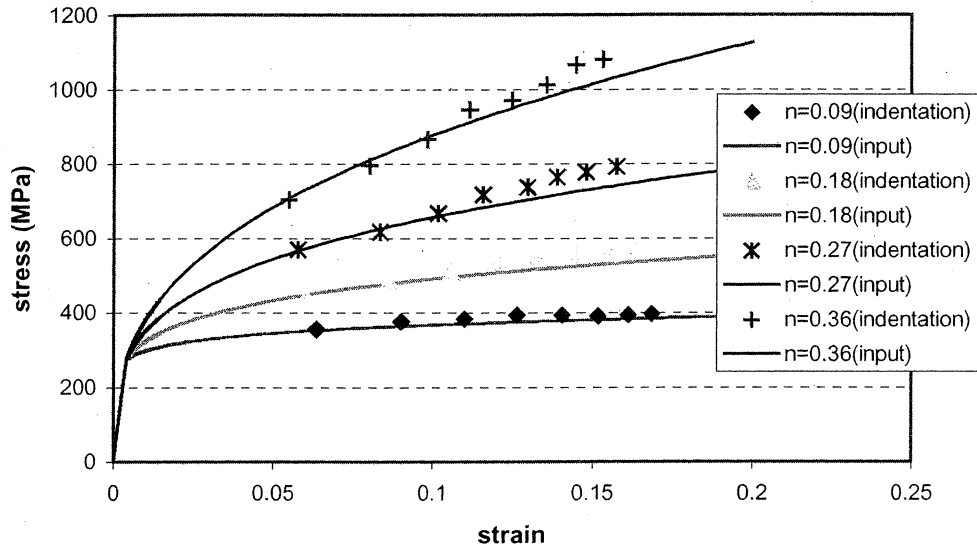


FIG. 8. Tabor's stress-strain relation for material set $E = 69$ GPa, $\sigma_y = 275$ MPa and $n = 0.09, 0.18, 0.27, 0.36$ respectively.

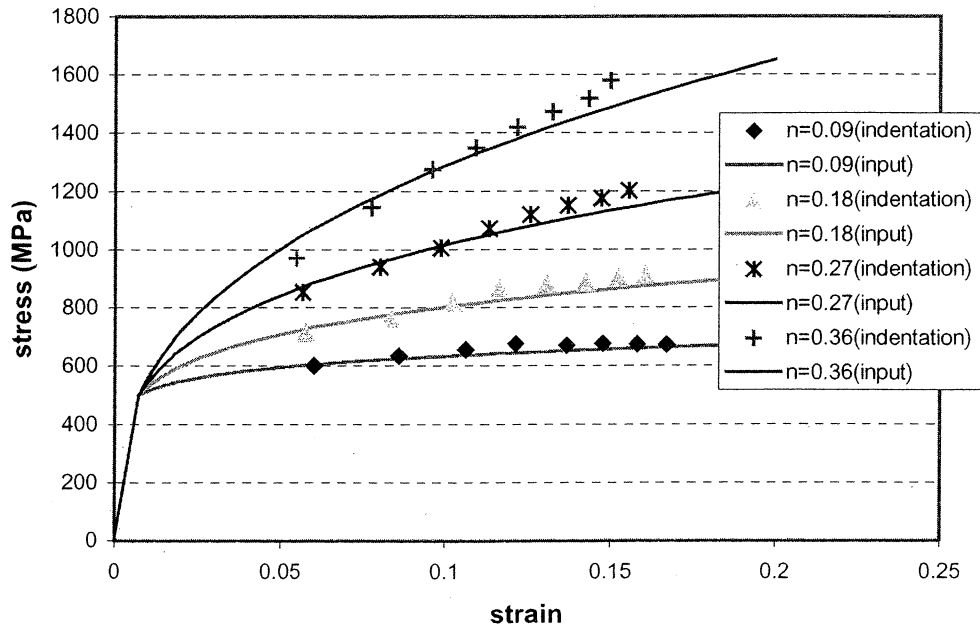


FIG. 9. Tabor's stress-strain relation for material set $E = 69$ GPa, $\sigma_y = 500$ MPa and $n = 0.09, 0.18, 0.27, 0.36$ respectively.

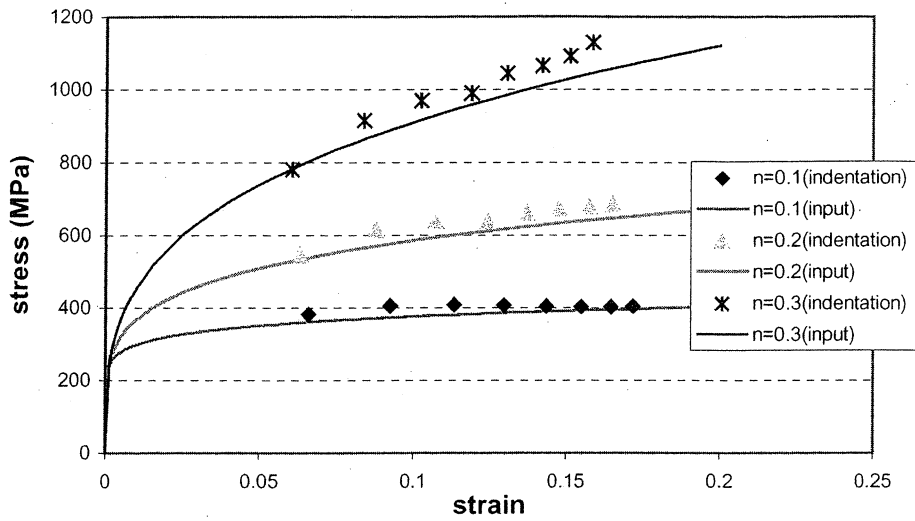


FIG. 10. Tabor's stress-strain relation for material set $E = 200$ GPa, $\sigma_y = 242$ MPa and $n = 0.1, 0.2, 0.3$ respectively.

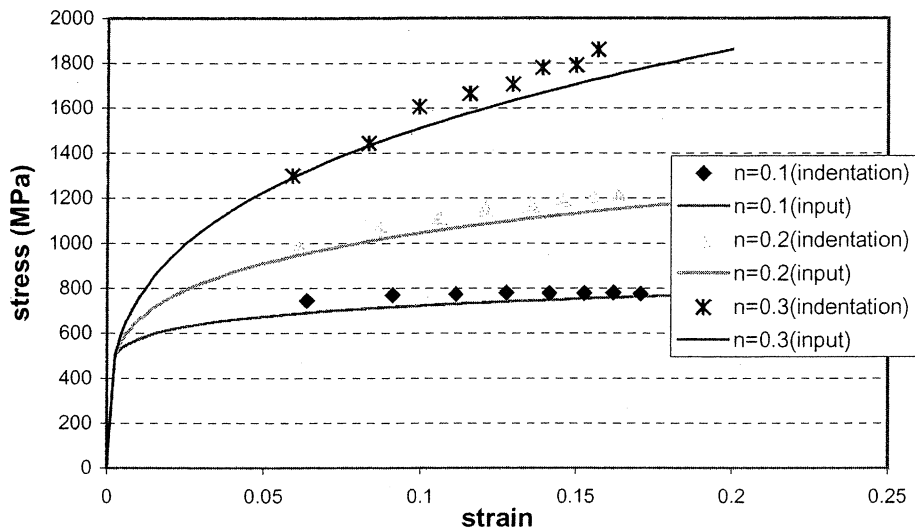


FIG. 11. Tabor's stress-strain relation for material set $E = 200$ GPa, $\sigma_y = 500$ MPa and $n = 0.1, 0.2, 0.3$ respectively.

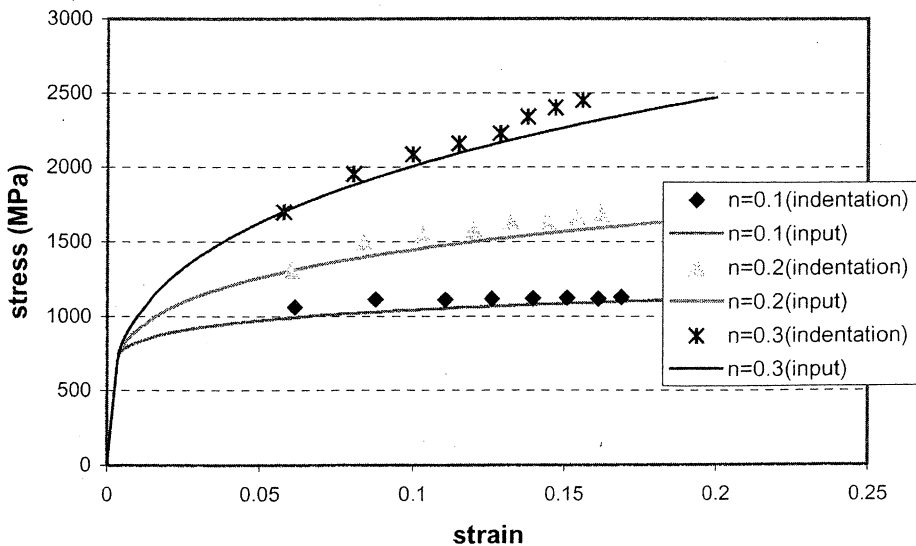


FIG. 12. Tabor's stress-strain relation for material set $E = 200$ GPa, $\sigma_y = 750$ MPa and $n = 0.1, 0.2, 0.3$ respectively.

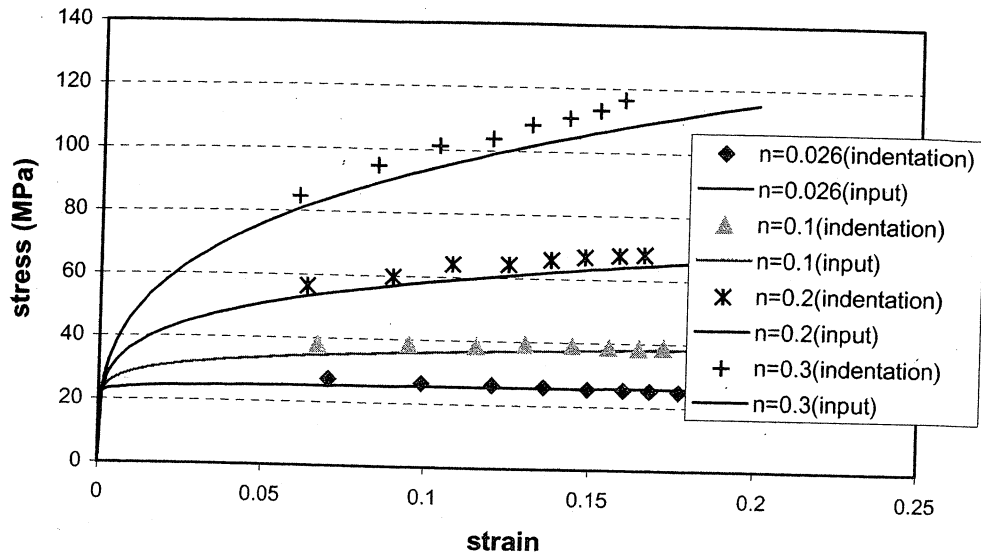


FIG. 13. Tabor's stress-strain relation for material set $E = 26.2$ GPa, $\sigma_y = 22.5$ MPa and $n = 0.026, 0.1, 0.2, 0.3$ respectively.

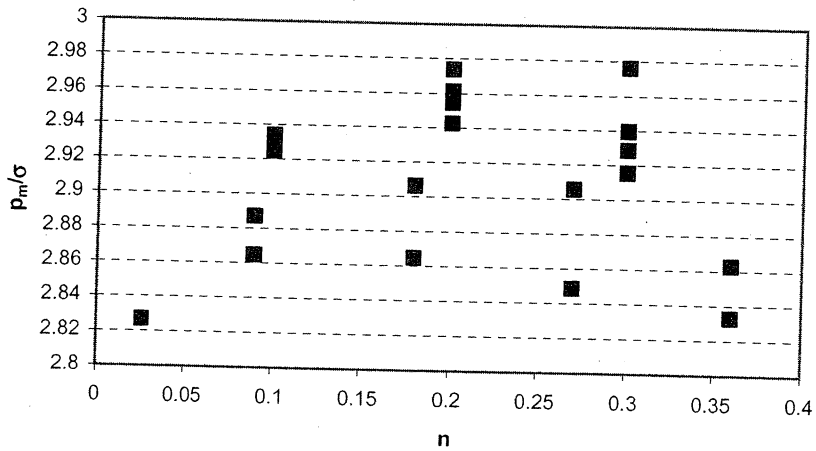


FIG. 14. p_m/σ fluctuation with respect to n value.

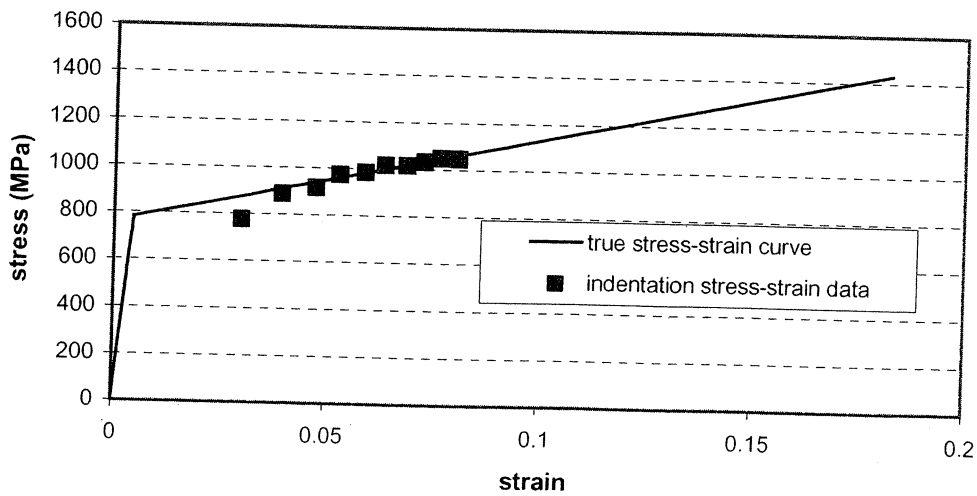


FIG. 15. Indentation stress-strain vs. true stress-strain of Inconel 783 alloy.

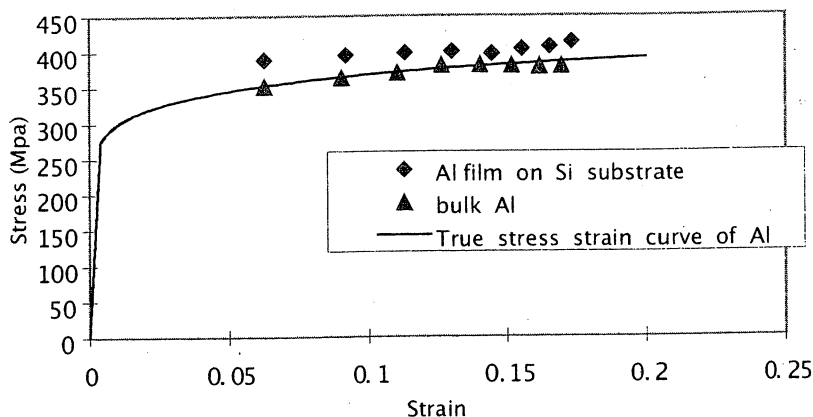


FIG. 16. Bulk Al and thin film Al on Si substrate.

7. THIN FILM SUBSTRATE SYSTEM

Computed stress-strain data of bulk aluminum as well as thin film Al on Si substrate, using Tabor's relation, is shown in Figure 16.

For the soft film on hard substrate case, Tabor's relation yields higher stress data. The effect of substrate cannot be ignored especially when the indentation depth is comparable with the coating thickness. The hard substrate effect will give a higher hardness (mean pressure p_m) value, which explains the thin film stress given by Tabor's relation being higher than the bulk stress.

As shown in Figure 17, even for bulk Si, the indentation stress-strain from Tabor's relation is not in good agreement with input stress-strain data. This can be attributed to the requirement of fully plastic condition for Tabor's relation. Inserting values for E and σ_y of Si into Eq. (3) gives $\epsilon_{\min} = 0.2 \sin[\tan^{-1}(30\epsilon_e)] = 0.144$ which is larger than most of the data shown in Figure 17. This is to show again that the Tabor indentation stress-strain data will only be in agreement with the input stress-strain curve for deeper indentation (large strain) and is not valid for shallow

indentation (small strain). For the thin film silicon on aluminum substrate, Tabor's prediction gets worse with increasing indentation depth. The predicted stress using Tabor's relation is much smaller than the actual stress. Due to the influence of the soft Al substrate, the deeper the indentation, the more discrepancies between Tabor's relation and true stress-strain curve are found. This result is expected, i.e., the soft Al substrate corresponds to a Meyer's hardness, which decreases with the increase of indentation depth.

It is concluded that the Tabor's relation cannot be directly employed to obtain true stress-strain curve for thin film materials. The effect of substrate cannot be neglected especially when the indentation depth is comparable with the film thickness [18].

8. CONCLUSIONS

Based on the modified Tabor formula, a simple indentation test procedure to obtain post-yielding stress-strain relationship of bulk ductile materials is established. FE simulations are performed to verify Tabor's empirical formulas. Stress-strain

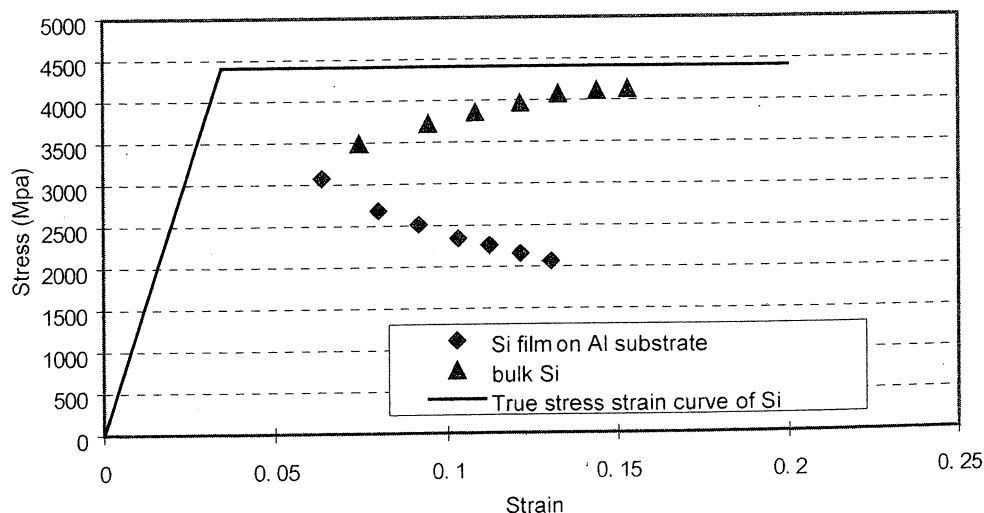


FIG. 17. Bulk Si and thin film Si on Al substrate.

curves calculated from the FE indentation simulations show good agreement with the input stress-strain curve. While adopting the definition of indentation strain as $\varepsilon_i = 0.2 d/D$, the indentation stress is modified to be $\sigma_i = p_m/\delta$, where δ is a value which fluctuates between 2.82 to 2.98. For thin film/substrate system, the indentation stress-strain data based on Tabor's relation are influenced by substrate and cannot be considered as intrinsic film mechanical properties, especially when the indentation depth is comparable with film thickness.

ACKNOWLEDGEMENT

The work was supported in part by DOE EPSCoR Program under contracts DE-FG02-01ER45899 and by the Office of Fossil Energy, Advanced Research Materials (ARM) Program, DOE, under contract DE-AC05-00OR22725 managed by UT-Battelle, LLC.

REFERENCES

1. <http://www.atc-ssm.com/library.html>
2. Murty, K. L., Mathew, M. D., Miraglia, P. Q., Shah, V. N., and Haggag, F. M., *Non-destructive Characterization of Materials in Aging Systems*, Materials Research Society, Penn, USA (1988).
3. Alcala, J., Giannakopoulos, A. E., and Suresh, S., "Continuous Measurements of load-penetration curves with spherical microindenters and the estimation of mechanical properties," *J. Mater. Research* **13**, 1390 (1998).
4. Field, J. S., and Swain, M. V., "Determining the mechanical properties of small volumes of material from submicrometer spherical indentations," *J. Mater. Research* **10**, 101 (1995).
5. Sneddon, I. N., "The relation between load and penetration in the axisymmetric boussinesq problem for a punch of arbitrary profile," *Int. J. Engng. Sci.* **3**, 47 (1965).
6. Doerner M. F., and Nix, W. D., "A method for interpreting the data from depth-sensing indentation instruments," *J. Mater. Research* **4**, 601 (1986).
7. Oliver, W. C., and Pharr G. M., "An improved technique for determining hardness and elastic modulus using load and displacement sensing indentation experiments," *J. Mater. Research* **7**, 1564 (1992).
8. Loubet, J. L., Georges, J. M., Marchesini, J. M., and Meille, G., "Vicker's Indentation Curves of Magnesium Oxide (MgO)," *J. Tribology* **106**, 43 (1984).
9. Laursen, T. A., and Simo, J. C., "A study of the mechanics of microindentation using finite elements," *J. Mater. Research* **3**, 618 (1992).
10. Tabor, D., *The Hardness of Metals*, Clarendon Press, Oxford, United Kingdom (1951).
11. Ahn, Jeong-Hoon, and Kwon, Dongil, "Derivation of plastic stress-strain relationship from ball indentations: Examination of strain definition and pileup effect," *J. Mater. Research* **16**, 3170 (2001).
12. Mata, M., Anglada, M., and Alcala, J., "Contact deformation regimes around sharp indentations and the concept of characteristic strain," *J. Mater. Research* **17**, 964 (2002).
13. Dao, M., Chollacoop, N., Van Vliet, K. J., Venkatesh T. A., and Suresh, S., "Computational modeling of the forward and reverse problems in instrumented sharp indentation," *Acta Mater* **49**, 3899-3918 (2001).
14. ABAQUS 6.3 version, manual.
15. Alcala, J., Barone, A. C., and Anglada, M., "The influence of plastic hardening on surface deformation modes around vickers and spherical indents," *Acta Materialia* **48**, 3451 (2000).
16. Bolshakov, A., and Pharr, G. M., "Influence of pileup on the measurement of mechanical properties by load and depth sensing indentation techniques," *J. Mater. Research* **13**, 1049 (1998).
17. Johnson, K. L., *Contact Mechanics*, Cambridge University Press, Cambridge, United Kingdom (1985).
18. Greco, F., and Luciano, R., "Analysis of the influence of incremental material response on the structural stability," *Mechanics of Advanced Materials and Structures* **12**(5), 363-377 (2005).